JOURNAL OF MECHANICAL ENGINEERING AND SCIENCES (JMES)
ISSN: 2289-4659 e-ISSN: 2231-8380
VOL. 16, ISSUE 3, 9081 – 9092
DOI: https://doi.org/10.15282/jmes.16.3.2022.10.0719

ORIGINAL ARTICLE

Investigation on the jet penetrated metal-diesel closed structures in condition of single-layer and multi-layer

C.F. Zhao[1,*], K.B. Zhang[1] and C.X. Zhao[2]

[1] School of Mechanical Engineering, Nanjing University of Science and Technology, Nanjing 210094, China.
Phone: +8615895890179
[2] School of Material Science and Engineering, Xiangtan University, Xiangtan, 411105, China.

ABSTRACT – For improving the protective performance of Armor, a multi-layer metal-diesel closed structure (MLMDCS) was proposed. The concept of equivalent layer number *n* and specific residual head velocity (SRHV) for describing the anti-jet penetration performance of single-layer metal-diesel closed structure (SLMDCS) and MLMDCS was put forward. The finite element simulation method by experimental verification was used to simulate the shaped charge jet (SCJ) penetrates the MLMDCS and SLMDCS. The simulation results show that when the equivalent layer number *n* (*n*>1) is the same, the residual head velocity of the jet through the MLMDCS is lower than that of the SLMDCS, and the time is longer than that of the SLMDCS. The energy consumption of jet in MLMDCS is more than that of in SLMDCS. The jet head becomes blunt after penetrating out the MLMDCS, but the head shape remains basically unchanged after the jet penetrates out the SLMDCS. The velocity streamline of diesel at the intersection of each layer in the MLMDCS is disordered, which forms local turbulence and disjoint phenomenon. The distribution positions of the diesel velocity streamline and pressure in the SLMDCS are basically the same. Compared with the SLMDCS, the MLMDCS has better anti-jet penetration properties, and the anti-jet penetration properties of the MLMDCS are better with the increase in the equivalent layer number. The research results provide a design reference for the new generation protective armor.

ARTICLE HISTORY
Received: 19th Mar. 2022
Revised: 16th July 2022
Accepted: 25th July 2022

KEYWORDS
Jet
Penetration
Metal-diesel
Closed structure
Anti-jet penetration
Numerical simulation

INTRODUCTION

With the development of science and technology, the rapid development of weapons and military industries, the contradiction between jet penetration and Armor protection is particularly prominent [1]. The anti-jet penetration performance of composite structures and materials has been the focus of researchers recently. Jia et al. [2] prepared an experimental study on the anti-jet penetration performance of four types of fabric-reinforced rubber composite target plates, such as Kevlar-49 and PBO, the function of fabric fiber in the process of anti-jet penetration were analyzed. Zu et al. [3] conducted an experimental research on the anti-penetration protection efficiency of rubber composite target plates and proved the anti-jet penetration performance of rubber composite armor. Sun et al. [4] studied the energy absorption law and the stress wave attenuation law of ceramic/foam aluminum/aluminum alloy composite structure anti-jet penetration by theoretical and numerical simulation.

In addition to reinforced target plates containing fabric fibers, composite target plates made of super-elastic rubber and laminated target plates of various solid substrates, there is a new type of target plate with solid-liquid combination. The solid-liquid target plate is characterized by filling material of the gap layer is liquid, which makes it have a different anti-jet penetration performance from the solid gap layer. White [5] and Andersson [6] carried out some experiments on anti-jet penetration of closed structures saturated with water or other liquids, the anti-jet penetration performance of liquid was preliminary proved. Zhang et al. [7] investigated the composite material rod jet penetrated a target in infinite water by numerical simulation. The composite rod jet with small head radius had a small resistance when it moved in water, whose contribution to the penetration of the target plate was significantly improved. For a closed structure composed of metal and liquid, Gao et al. [8], Zhao et al. [9-13], Shan et al. [14] and Zhao et al. [15] obtained the anti-jet penetration capabilities of the single cell closed structure (SLMDCS) by steady penetration theory, finite element numerical simulation and residual penetration depth experiments and other methods. The research filed included liquid properties, size effects, penetration angles and so on. Guo et al. [16] studied the anti-jet penetration performance of transverse multi-cell structure filled with liquid, and some theoretical and experimental results were obtained. Zu et al. [17] studied the anti-jet penetration performance of the transverse multi-cell structure filled with liquid using experimental methods, especially discussed the influence of the filled liquid properties (such as dynamic viscosity, density and sound velocity) on the the jet. It was pointed out that the radial convergence effect of liquid greatly interfered with the residual penetration capability of the jet. However, the anti-penetration performance of the SLMDCS is pretty limited, and how to improve its anti-penetration capability is worthy of attention. On this basis, the MLMDCS emerged at the historic moment.

To understand the anti-penetration performance of MLMDCS, the finite element fluid-solid coupling ALE method verified by experiments was used to simulate the anti-penetration performance of MLMDCS from the aspects of jet

*CORRESPONDING AUTHOR | C.F. Zhao | ✉ lackychang@njust.edu.cn

residual head velocity and head shape, pressure and deformation of the closed structure, diesel motion state and liquid energy change, etc. Furthermore, compared with the multi-layer equal height structure, the anti-penetration performance of the SLMDCS was also studied.

DESIGN OF STRUCTURE

The literature [8-17] had proved the anti-penetration performance of the LC4 aluminum alloy-diesel closed structure. The materials and the geometric dimensions of the structure were used by referring to them. In Figure 1 (a), for vertical penetration of single-layer metal-diesel protective armor, the ways to improve its protective performance are to increase the height of the closed structure and replace the filled liquid. When the material is determined, the method for increasing the armor protection capability is only increasing the height of the closed structure, which will bring the consequences of increased mass and volume. Based on this, in the case of insufficient protection performance of a single-layer closed structure, the composite form of multi-layer metal-diesel can be used to improve the anti-penetration performance without increasing the height of the closed structure. In other words, it only changes the internal composition of the closed structure. Therefore, the height of the multi-layer metal-diesel composite closed structure is the same as the height of the single-layer closed structure in this paper. The purpose is to verify which structure has better anti-penetration performance at the same height.

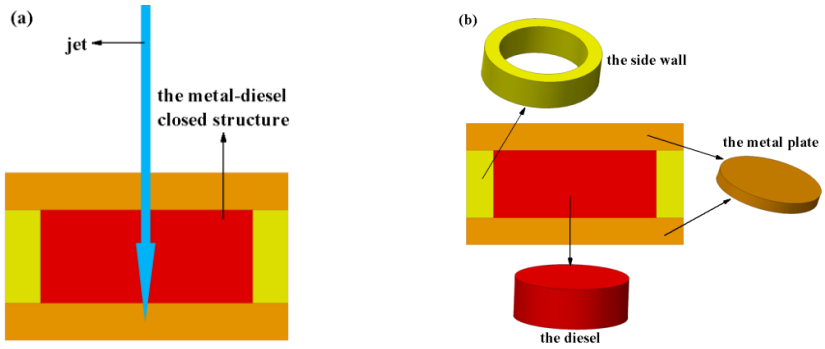

Figure 1. 1/2 model of SLMDCS: (a) the model of jet penetration SLMDCS and (b) the combination of closed structure

The SLMDCS is regarded as a base, which is composed of a layer of diesel, two metal plates and a side wall. It's shown in Figure 1. In fact, the closed structure is welded to form a whole. For MLMDCS of different heights, the equivalent layer number is defined as n (n is a positive integer N^*), which means a MLMDCS is composed of n bases. The SLMDCS with different heights originally had only one layer, but the geometric sizes are different from the base. To facilitate the description in comparative analysis, the equivalent layer number n is also used to describe its height. When the equivalent layer number n is the same, the height of the SLMDCS is the same as the height of the MLMDCS. The equivalent defined here is the equivalent in geometric height, and the structure mass and diesel volume are not equal. For example, when the equivalent layer number n is 3, the corresponding structure is shown in Figure 2.

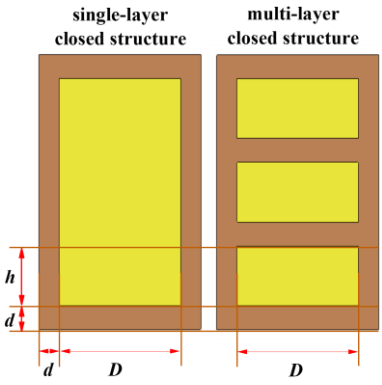

Figure 2. 1/2 model of SLMDCS and MLMDCS (n=3), explaining the equivalent layer number

For a single-layer base, the mass of the side wall is m_w, and the mass of the metal plate is m_p. Thereby, the mass of the diesel m_d is as follows.

$$\begin{cases} m_{\mathrm{w}} = \rho_{\mathrm{w}} \dfrac{\pi[(D+2d)^2 - D^2]}{4} h \\ m_{\mathrm{p}} = \rho_{\mathrm{p}} \dfrac{\pi(D+2d)^2}{4} d \\ m_{\mathrm{d}} = \rho_{\mathrm{d}} \dfrac{\pi D^2}{4} h \end{cases} \tag{1}$$

where ρ_{w}, ρ_{p} and ρ_{d} are the density of the side wall, metal plate and diesel. Obviously, $\rho w=\rho_{\mathrm{p}}$.
For the SLMDCS with an equivalent layer number of n, its mass m_{s} is:

$$m_{\mathrm{s}} = [n + (n-1)\frac{d}{h}](m_{\mathrm{w}} + m_{\mathrm{d}}) + 2m_{\mathrm{p}} \tag{2}$$

For the MLMDCS with an equivalent layer number of n, its mass m_{m} is:

$$m_{\mathrm{m}} = n \cdot (m_{\mathrm{w}} + m_{\mathrm{d}}) + (n+1) \cdot m_{\mathrm{p}} \tag{3}$$

According to Ref. [8-15], d=5 mm, D=30 mm, h=12.5 mm. By calculation, m_{w}=19.03 g, m_{p}=17.40 g and m_{d}=7.39 g. Hence, the mass of the base is 61.22 g. By combining Eqs. (2) and (3), the relationship between the mass of the SLMDCS and MLMDCS and the equivalent layer number n can be obtained, which is shown in Figure 3 below.

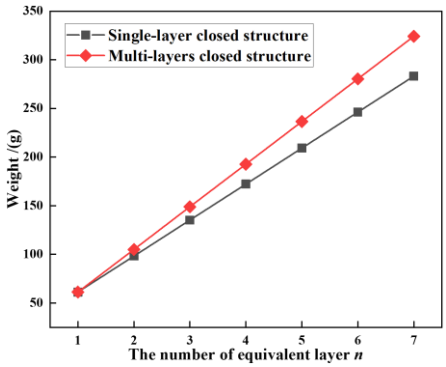

Figure 3. The relationship between the mass and equivalent layer number of closed structures

Generally, when judged the anti-penetration performance of an armor, its mass and volume need to be considered. Since the single layer and multi-layer cell structures mentioned in this paper have the same volume to the external space, only the mass is considered. The residual head velocity can be used to evaluate the interfered degree to the jet when the jet penetrates through the closed structure. Therefore, the specific residual head velocity (SRHV) is defined to measure the anti-jet penetration performance of the two structures. The calculation method of SRHV is as follows.

$$SRHV = \frac{v_{\mathrm{j}}}{m} \tag{4}$$

where v_{j} is the residual head velocity of the jet, and m is the mass of the closed structure.

THEORETICAL EQUATIONS

Motion Equation of Diesel

The MLMDCS is a series form of base. For the n-th (n>1) base, the space is very limited when the jet does not penetrate the n+1 layer base. After the space between the two bases is penetrated, the jet and the upper layer diesel flow together into the next layer, and a large amount of instantaneous accumulation in the next base. Further, high-pressure diesel transmits the force to the closed structure to deform it.

After the jet penetrates through the first base, the diesel in the first base will flow into the second base with the jet, and so on, until the jet leaves the last base. Assuming that the metal layer is the control surface, the diesel in the closed structure is the control body, and the motion velocity and pore area of the diesel on the control surface are V_n and A_n. Then, the mass conservation equation of the control body in the n-th base is:

$$\sum_n (V_n A_n)_{out} = \sum_n (V_n A_n)_{in} \tag{5}$$

For diesel micro-elements, if V_n is the vector of the diesel velocity v_n, we ignore the volume force f of the diesel micro-elements. For Newtonian fluids with zero pressure, the differential equation for momentum conservation of diesel micro-element clusters can be expressed as:

$$\begin{cases} \dfrac{\partial V_n}{\partial t} = \dfrac{\nabla \cdot \sigma}{\rho} \\ \sigma = 2\mu\dot{\varepsilon} \end{cases} \tag{6}$$

where σ is the second-order symmetrical stress tensor, and ρ is the diesel density. μ is the volume viscosity, and $\dot{\varepsilon}$ is the strain rate tensor.

For adiabatic processes, the energy conservation equation considering the internal energy e of the diesel is:

$$\frac{\partial}{\partial t}(e+\frac{|V|^2}{2})+V\cdot\nabla(e+\frac{|V|^2}{2})=\frac{\nabla\cdot(V\cdot\sigma)}{\rho} \tag{7}$$

The jet penetrates into MLMDCS is a typical large-deformation nonlinear multi-physics fluid-solid interaction analysis. Arbitary Lagrangian and Eulerian method (ALE) is required for the finite element calculation. In the ALE algorithm, the three major conservation equations are redefined according to the reference point. If the reference point is Ψ, then the ALE satellite derivative of the particle Ω is as follows [18-19].

$$\begin{cases} \left.\dfrac{\partial N}{\partial t}\right|_{\Omega} = \left.\dfrac{\partial N(\Psi,t)}{\partial t}\right|_{\Omega} + c_i \dfrac{\partial N}{\partial \Omega_i} \\ c_i = u_i - w_i \end{cases} \tag{8}$$

where t is time, N is a certain physical parameter, and c_i is the convection velocity. u_i is the matter velocity of the particle Ω, and w_i is the matter velocity of the reference point Ψ.

Based on the ALE satellite derivative, the ALE control equation can be derived as follows:
Mass conservation equation

$$\left.\frac{\partial \rho}{\partial t}\right|_{\Psi} + c_i \frac{\partial \rho}{\partial \Omega_i} + \rho \frac{\partial v_i}{\partial \Omega_i} = 0 \tag{9}$$

Momentum conservation equation

$$\rho \left.\frac{\partial v_i}{\partial t}\right|_{\Psi} + \rho c_j \frac{\partial v_i}{\partial \Omega_j} = \frac{\partial \sigma_{ij}}{\partial \Omega_j} + \rho f_i \tag{10}$$

Energy conservation equation

$$\rho \left.\frac{\partial e}{\partial t}\right|_{\Psi} + \rho c_i \frac{\partial \rho}{\partial \Omega_j} = \sigma_{ij} \frac{\partial v_i}{\partial \Omega_j} - \frac{\partial q_i}{\partial \Omega_i} \tag{11}$$

where ρ is the density of matter, fi is the body force per unit mass, and σ_{ij} is the Cauchy stress tensor. e is the internal energy per unit mass, and q_i is the heat flux.

Constitutive Equation of Materials

The penetration model includes five parts: explosive, charge cover, air, metal structure and filled liquid. Among them, the Jones-Wilkins-Lee equation of state is used to describe the pressure p of explosive gas [20], that is,

$$\begin{cases} p = A(1-\dfrac{\omega\eta}{R_1})^{\frac{R_1}{\eta}} + B(1-\dfrac{\omega\eta}{R_2})^{\frac{R_2}{\eta}} + \omega\eta E \\ \eta = \dfrac{\rho_r}{\rho} \end{cases} \tag{12}$$

where η is the relative density, which is defined as the ratio of the detonation gas density ρ_r to the initial explosive density ρ. E is the specific internal energy of the high-energy explosive. A, B, R_1, R_2 and ω are material coefficients obtained by fitting the experimental data.

The cover and metal structure are described by Johnson-Cook material model and Gruneisen state equation. The Johnson-Cook equation [21] is:

$$\begin{cases} \sigma_y = (A + B\bar{\varepsilon}^{p^n})(1 + C ln\dot{\varepsilon}^*)(1 - T^{*^m}) \\ \dot{\varepsilon}^* = \dfrac{\dot{\bar{\varepsilon}}^p}{\dot{\varepsilon}_0} \\ T^* = \dfrac{T - T_r}{T_m - T_r} \end{cases} \tag{13}$$

where σ_y is the equivalent plastic stress. A, B, C, n, and m are material parameters. $\bar{\varepsilon}^p$ is the equivalent plastic strain, and $\dot{\varepsilon}^*$ is the equivalent plastic strain rate. $\dot{\varepsilon}_0$ generally takes 1.0 s-1. T^* is the melting temperature, Tr is the room temperature and Tm is the melting temperature of the material in the normal state.

The Gruneisen compression and expansion state equation [22] is:

$$\begin{cases} p_{\text{compress}} = \dfrac{\rho_0 C^2 \mu[1+(1-\frac{\gamma_0}{2})\mu - \frac{a}{2}\mu^2]}{[1-(S_1-1)\mu - S_2\frac{\mu}{1+\mu} - S_3\frac{\mu^3}{(1+\mu)^2}]} + (\gamma_0 + a\mu)E \\ p_{\text{expand}} = \rho_0 C^2 \mu + (\gamma_0 + a\mu)E \\ \mu = \dfrac{\rho}{\rho_0} \text{-} 1 \end{cases} \tag{14}$$

where p_{compress} is the pressure of compression state, p_{expand} is the pressure of expansion state, and C is the intercept of the shock wave velocity-particle velocity curve. S_1, S_2 and S_3 are the coefficients of the slope of the shock wave velocity-particle velocity curve. γ_0 is the Gruneisen constant, and a is the first-order volume correction of γ_0. μ is the relative density, which is defined as the ratio of the current density ρ to the initial density ρ_0 minus 1.

The diesel is described by the NULL empty material model and the Gruneisen state Eq. (14). The air is also described by the NULL empty material model, but the state equation is described by linear polynomial Linear_Polynomial. The linear polynomial equation [22] is:

$$\begin{cases} p = C_0 + C_1\mu + C_2\mu^2 + C_3\mu^3 + (C_4 + C_5\mu + C_6\mu^2)E \\ \mu = \dfrac{\rho}{\rho_0} - 1 \end{cases} \tag{15}$$

where C_0, C_1, C_2, C_3, C_4, C_5 and C_6 are constants. μ is the relative density, which is defined as the ratio of the current density ρ to the initial density ρ_0 minus 1. E is the internal energy per unit volume.

FINITE ELEMENT SIMULATION

Simulation Model

The finite element mesh model used in the simulation includes five parts: JH-2 explosive, copper cover, air, 0# diesel, closed structure of LC4 aluminum alloy with equal wall thickness. Among them, explosive, air, cover and diesel are modeled by three-dimensional Euler grid, and the metal structure is modeled by three-dimensional Lagrange grid. The Φ56 mm charge is made with a cone angle of 60°, and the charge is shell-free. The charge height is 73 mm, the cover thickness is 1 mm. The distance between the bottom of the charge cover and the top of the closed structure (explosion height) is 80 mm. The 5-layer metal-diesel closed structure is shown in Figure 4. During the research, the explosion height is maintained. The simulation conditions are divided into a SLMDCS and MLMDCS, and n=1 to 5, so there are a total of 9 simulation conditions.

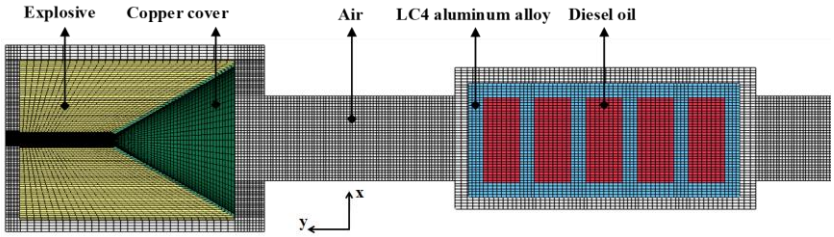

Figure 4. Finite element mesh model of MLMDCS (*n*=5)

Verification of Simulation Methods

The LS-DYNA finite element software was used to simulate the jet penetrates the metal-diesel closed structure with an equivalent layer number *n* of 2. The parameters used in the constitutive equation of the material were referenced in [8]. The simulation results are shown in Figure 5. The morphology of the jets taken by the two pulse X-ray machines at different times is shown in Figure 6, and the experimental results and comparison with the simulation results are shown in Table 1. According to the comparison results between experiments and simulations, the relative errors in the residual head velocity and the residual penetration depth are all within acceptable ranges. Hence, it is considered that the simulation models and simulation methods are suitable, the simulation results obtained using the method are reliable.

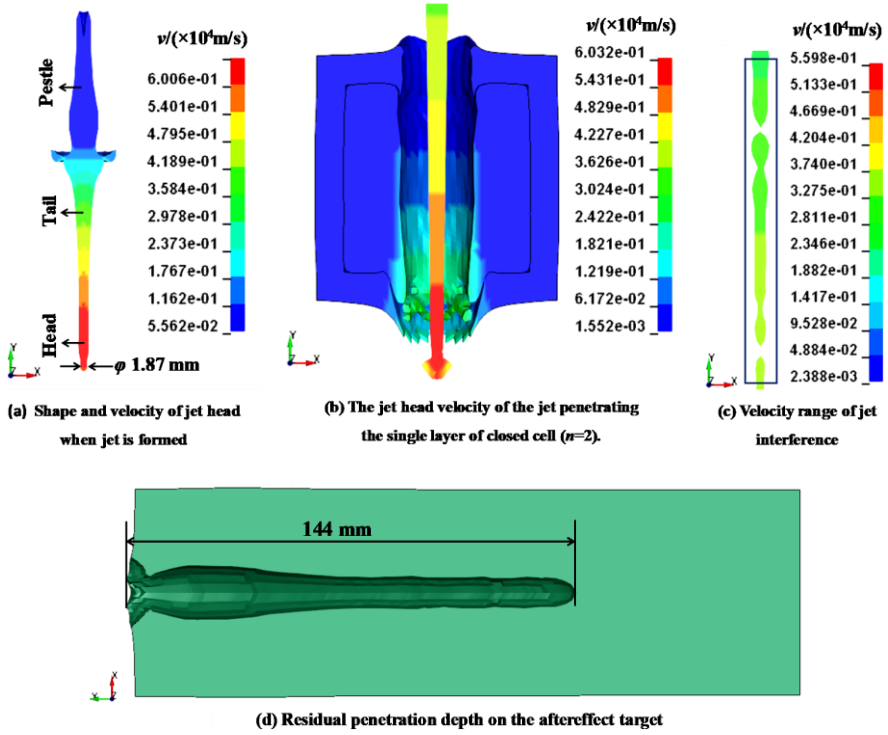

Figure 5. Simulation results of the jet penetration into a SLMDCS (*n*=2)

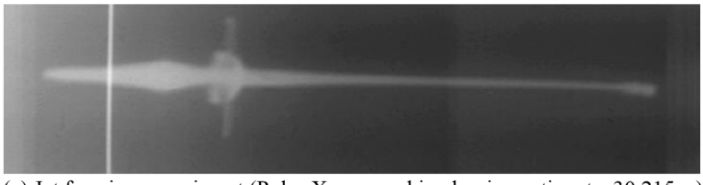

(a) Jet forming experiment (Pulse X-ray machine luminous time t_1=30.215μs)

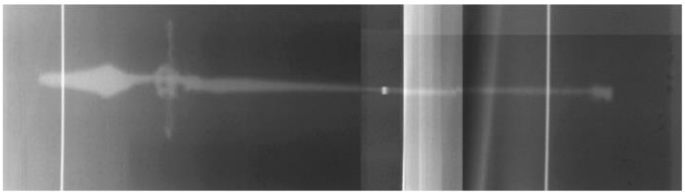

(b) Jet forming experiment (Pulse X-ray machine luminous time t_2=50.393μs)

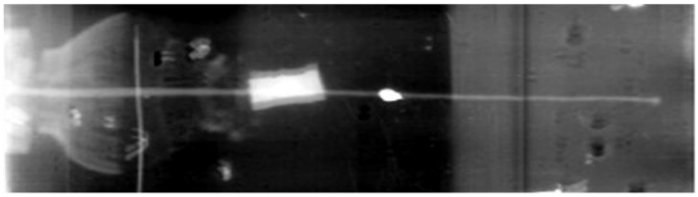

(c) Jet penetration experiment (Pulse X-ray machine luminous time t_1=50μs)

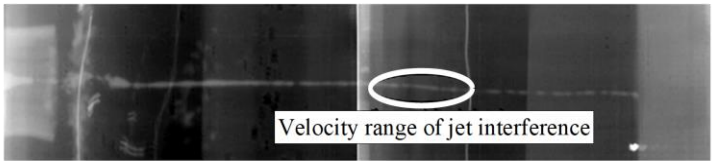

(d) Jet penetration experiment (Pulse X-ray machine luminous time t_2=80μs)

Figure 6. Experimental results of jet penetration closed structure (n=2) [23]

Table 1. Comparison of simulation results with experimental results

Compare content	Head velocity when jet forms /(m/s)	Tail velocity when jet forms /(m/s)	Head radius /(mm)	Residual head velocity /(m/s)
Simulation	6 612	1 162	1.87	6 032
Experiments	6 510	1 189	2.00	6 038
Relative error	1.6%	2.3%	6.5%	0.1%

Table 1. continued

Compare content	Interference velocity range		Residual penetration depth /(mm)
	Minimum velocity /(m/s)	Maximum velocity /(m/s)	
Simulations	2 750	3 640	144
Experiments	2 788	3 247	169
Relative error	1.4%	12.1%	14.8%

SIMULATION RESULTS AND DISCUSSIONS

Velocity of Jet Head

To a large extent, the penetration capability of the jet can be measured by the head velocity (show in figure as v). The higher the jet head velocity is, the stronger the penetration capability is. According to the simulation results (Figure 7), with the equivalent layer number n increases, the jet head velocity of penetrating through the metal-diesel closed structure shows a downward trend. However, the velocity of MLMDCS decreases faster, which indicates that MLMDCS has a better capability to interfere with jet. From the Figure 7(g), the SRHV of the MLMDCS is lower than that of the SLMDCS, but the gap maintains unchanged with the increase in n. However, in Figure 3, as the increase of the equivalent layer number n, the mass gap between the MLMDCS and the SLMDCS becomes much larger and larger. However, the SRHV difference in Figure 7(g) is unchanged, which further proves the excellent anti-jet penetration performance of the MLMDCS. The literature [22] pointed out that the main reason for the interference of jet penetrates the diesel-filled closed structure is the radial convergence of the diesel. As can be seen in Figure 7(a) to (e), the radial convergence of the diesel in the MLMDCS is discontinuities. In the SLMDCS, the radial convergence of the diesel increases with the increase in the number of equivalent layer, which shows the convergence-expansion shape. The reason for the significant difference between single layer and MLMDCS diesel radial convergence is whether has an intermediate metal barrier. The barrier obstructs diesel flow so that causes a drastic change in the movement.

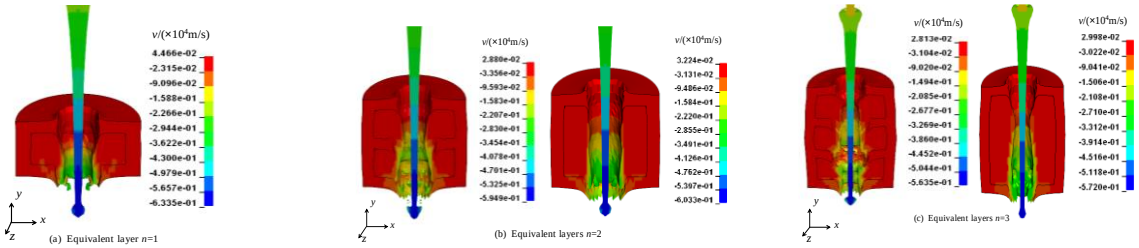

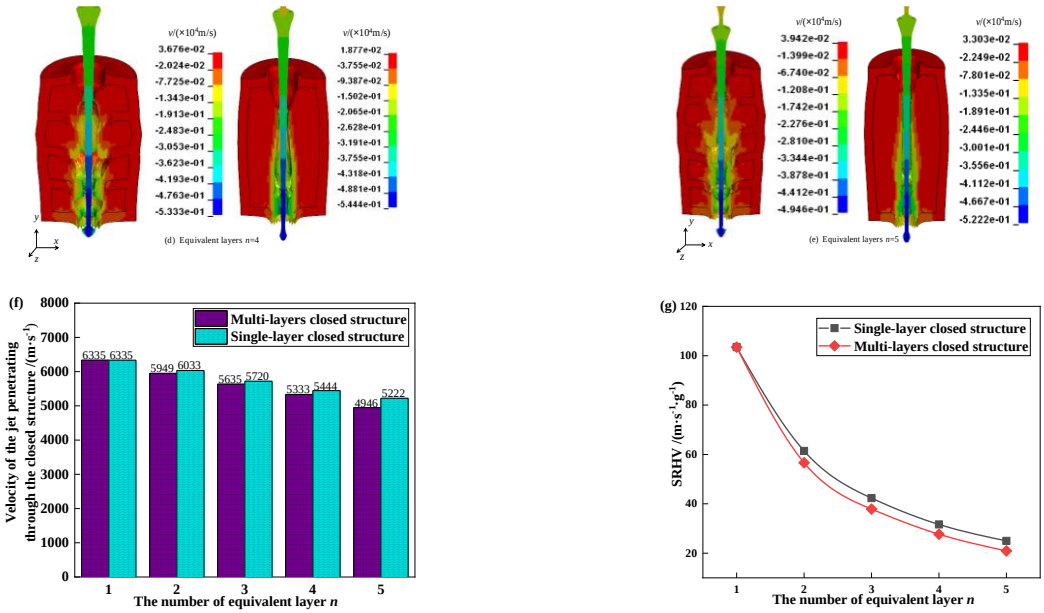

Figure 7. Velocity of the jet penetrates through metal-diesel closed structure with different *n*

Pressure Distribution of Closed Structure and Penetration Time

The diesel driven by the shock wave of the jet moves toward the closed structure, and after reflecting on the wall of the closed structure. It converges radially and interferes with the jet, so the pressure distribution of the closed structure reflects the position and strength of the shock wave when it reaches the wall. From Figure 8, it can be seen that the pressure distribution of the MLMDCS is relatively uniform, and there is no obvious concentration phenomenon. The opening hole radius on the metal layer first increases and then decreases. The SLMDCS has a "pressure ring" on the inner wall surface. With the equivalent layer number *n* increases, the amplitude of the pressure ring decreases. The distribution range becomes smaller, and it gradually approaches the bottom surface. The shock wave is repeatedly reflected by the intermediate metal barrier when it moves in the MLMDCS. With the increase of time, the exponentially decaying shock wave is basically consumed when the jet reaches the bottom of the closed structure. In the SLMDCS, the effect of the first wave on the closed structure is obvious, and the subsequent wave intensity gradually decreases. The macroscopic physical phenomenon is that diesel accumulates with the jet's movement to the bottom of the closed structure, which causes the pressure at the bottom of the closed structure to increase. However, in the MLMDCS, due to the disturbance and resistance of the intermediate metal barrier, the diesel is "trapped" in the respective layers. Hence, it has no large accumulation in the last base.

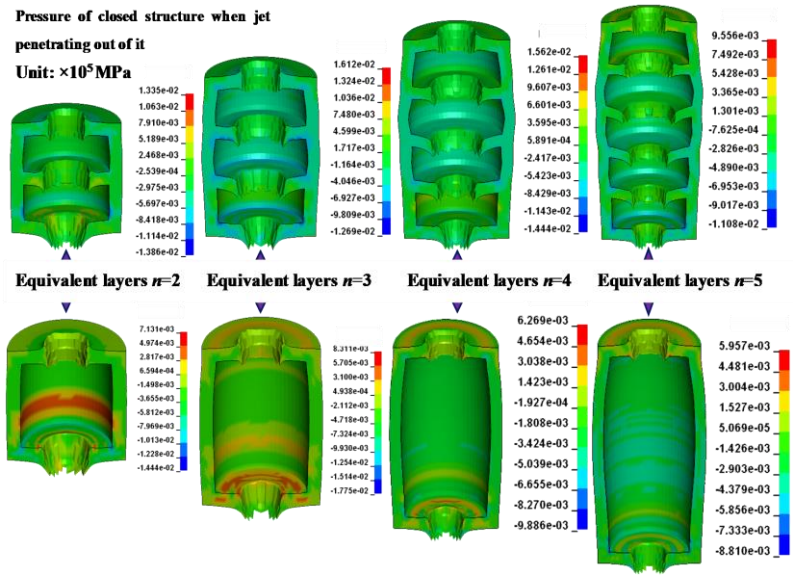

Figure 8. Pressure of closed structure when jet penetrates out of it [15]

According to Figure 9, it can be seen that the time of the jet penetrates through the metal-diesel closed structure increases with the increase in the equivalent layer number *n*, and the time of the jet penetrates through the MLMDCS is

longer than that of the SLMDCS. These results are confirmed by the low residual head velocity when the jet is out of the metal-diesel closed structure, which further shows that the capability of interfering jet with MLMDCS is better than SLMDCS.

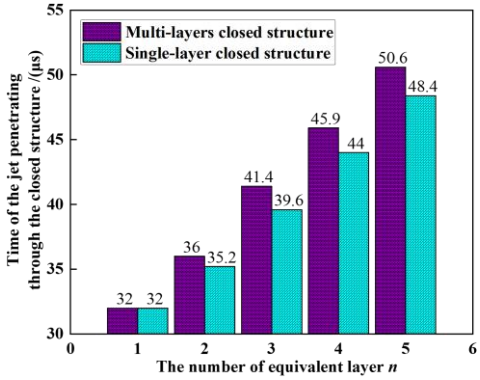

Figure 9. Time of the jet penetrates through the SLMDCS and MLMDCS

Deformation of Jet Head

A slender head jet and stout tail pestle rod are formed after the axial compression of the cover by explosive gas. The jet head diameter is smaller than the neck and tail when the jet head is not disturbed. As can be seen from Figure 10, as the equivalent layer number *n* increases, the shape of the jet head after penetrating the single-layer and MLMDCS is obviously different, which are similar to the "bowling" and "inverted triangle" shape, respectively. The metal layer can be regarded as fluid when the high-speed jet penetrates into the metal plate. However, with the jet head velocity decreases, the strength of the metal layer becomes apparent. The multi-layer metal-diesel combination forms a rigid-flexible coupling model, which better interferes with the jet and makes the jet head micro-elements have a velocity difference to become blunt. Therefore, the MLMDCS contributes more to the deformation of the jet head than that of the SLMDCS, and the shape of the jet head can be used as another standard to measure the interference of the jet.

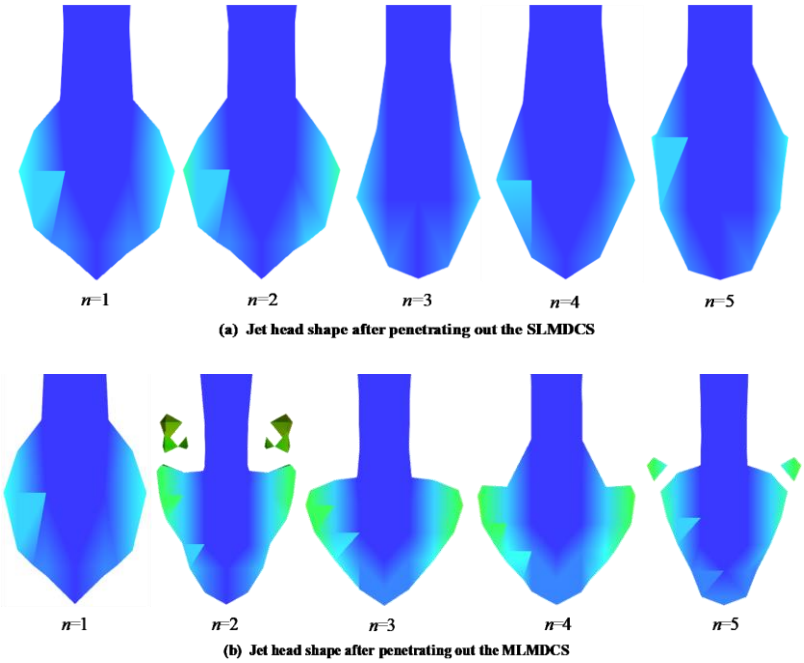

Figure 10. Jet head shape at the moment of Time=42 μs

Velocity Streamlines of Diesel and Energy Curves of Jet

After the jet penetrates into the closed structure, the disturbed diesel will converge radially and accompany the jet to move. Due to the existence of an intermediate metal barrier in the MLMDCS, the next layer of diesel remains stationary when the jet penetrates the previous layer of diesel. Therefore, the diesel in each layer of the closed structure can theoretically produce radial convergence. However, the action time is short, and the shock wave decays and moves particularly fast. It can be considered that there is only one shock wave, so the diesel in the upper layer poured into the next closed structure with the jet before converging, and so on. According to Figure 11, it can be found that the pressure and velocity of the diesel in the MLMDCS are all in the last base. The velocity streamlines at the diesel junction between

the layers are disordered to form local turbulence. However, the diesel in the SLMDCS, it shows a consistent phenomenon, the pressure at the bottom of the diesel is the highest.

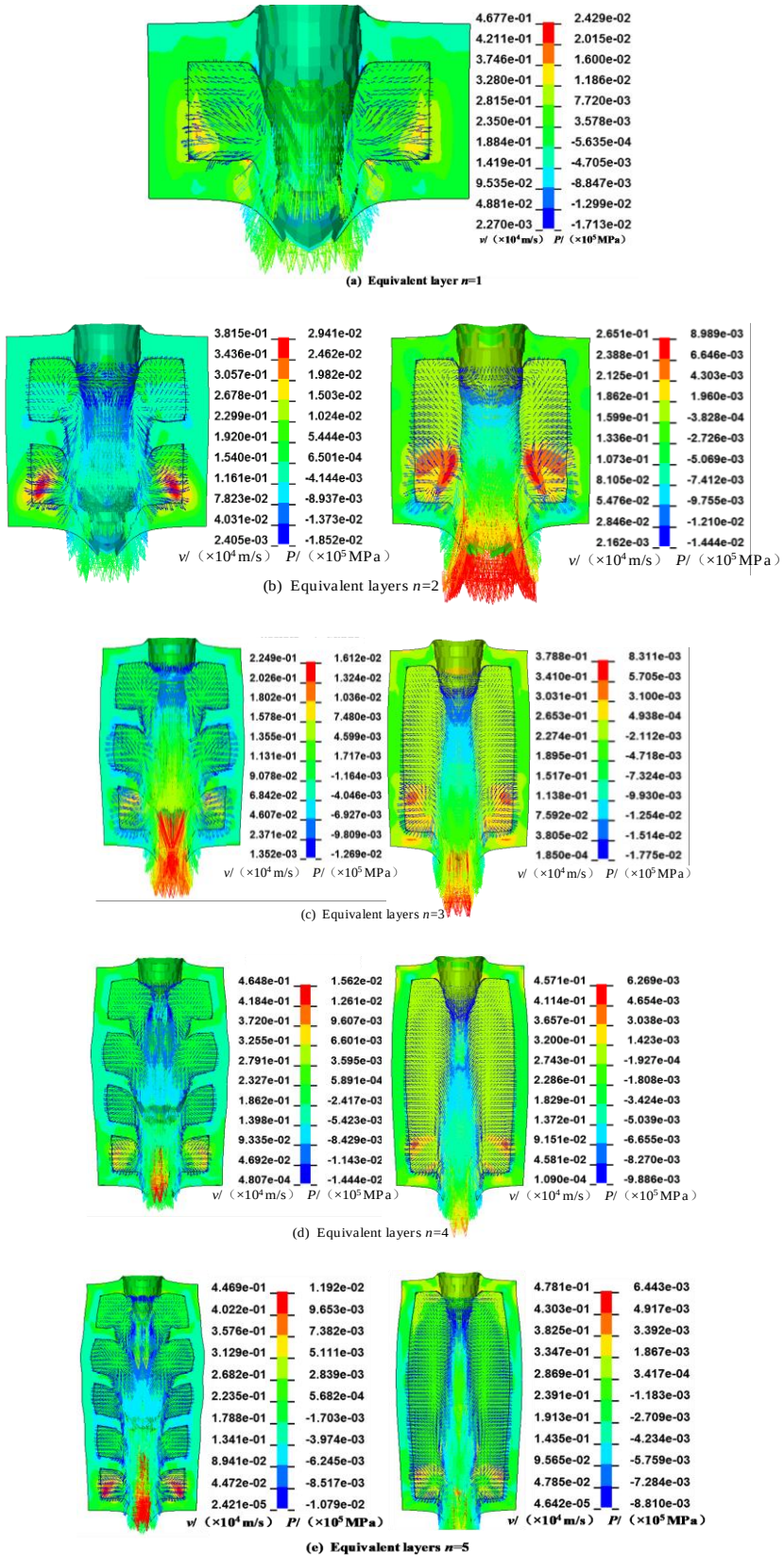

Figure 11. Pressure and velocity streamlines of diesel in the MLMDCS and SLMDCS

The capability of the metal-diesel closed structure to anti-jet penetration is also reflected in energy consumption. The lower the energy of the jet when it through the metal-diesel closed structure, the greater knterference occurred and the more energy consumed. The kinetic energy change curve Figure 12 shows that with the same of equivalent layer number *n*, the MLMDCS consumes more energy of the jet, which corresponds to the extension of the penetration time. The

reduction of the jet residual head velocity, and the jet head to blunt, which together shows the superior capability of the MLMDCS to interfere with the jet.

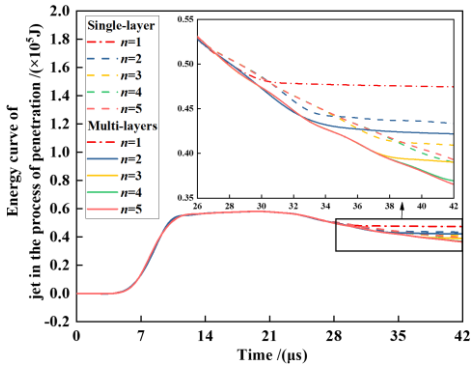

Figure 12. Energy curve of jet in the process of penetration

CONCLUSION

In view of the lack of anti-jet penetration performance of single-layer metal-diesel composite armor, a multi-layer metal-diesel composite closed structure was proposed. By using suitable simulation method and effective simulation model, the single-layer and MLMDCS with different heights (different equivalent layer *n*) were simulated and studied. Some conclusions were drawn as follows. When the total height of the metal-diesel closed structure is the same, the residual head velocity of the jet through the MLMDCS is lower than that of the SLMDCS, the time of the jet through the MLMDCS is longer than that of the SLMDCS, and the MLMDCS consume more jet energy. The jet head becomes blunt after penetrating the MLMDCS, and the shape of the jet head after penetrating the SLMDCS is basically unchanged. The MLMDCS forms local turbulence and disjoint phenomenon due to the intermediate metal barrier, and the flow at the junction of each layer of diesel is disordered. However, the SLMDCS has the same distribution position of diesel streamline and pressure. Compared with SLMDCS, MLMDCS has a better anti-penetration capability, and its anti-penetration performance will be better with the equivalent layer number increases.

ACKNOWLEDGEMENTS

This work was financially supported by the China Scholarship Council (202106840033, corresponding to Changfang Zhao), the Postgraduate Research & Practice Innovation Program of Jiangsu Province of China (KYCX19_0327, corresponding to Changfang Zhao), and the Excellent Doctor Training Fund of Nanjing University of Science and Technology (Awarded in 2022, corresponding to Changfang Zhao). Furthermore, assistance in finite element analysis from Prof. Xudong Zu in the School of Mechanical Engineering, Nanjing University of Science and Technology was acknowledged.

CONFLICT OF INTEREST

The authors have no relevant financial or non-financial interests to disclose.

REFERENCES

[1] F. Y. Wang, "The development of armor fence," *Journal of Test and Measurement Technology*, vol. 1, no. 02, pp. 144-147, 2002.

[2] X. Jia, Z. X. Huang, X. D. Zu et al., "Protective effect of woven fabric reinforced rubber composite target against shaped charge jet," *Acta Materiae Compositae Sinica*, vol. 29, no. 06, pp. 66-72, 2012.

[3] X. D. Zu, Z. X. Huang, X. H. Gu, "Experiment study of defense efficiency about rubber composite armor against shaped charge jet," *Journal of Ballistics*, vol. 23, no. 01, pp. 54-57, 2011, doi: 10.1097/MCC.0b013e328344b397.

[4] D. Sun, R. J. Gou, "Analysis of resisting to the linear jet penetration of the ceramic/aluminum foam/aluminum alloy and structure optimization," *Initiators & Pyrotechnics*, no. 05, pp. 32-36, 2016.

[5] J. J. White, J. M. Wahll, "Shaped charge jet interactions with liquids," *Proceedings of the 6th International Symposium on Ballistics. Orlando, FL: International Ballistics Society*, pp. 305-311, 1981.

[6] G. Andersson, S. Karlsson, A. Watterstam, "Shaped charge jet interaction with confined water," *Proceedings of the 17th International Symposium on Ballistics. Midrand, South Africa: The South Africa Ballistics Organisation*, pp.183-190, 1998.

[7] C. H. Zhang, F. Zhang, Z. J. Wang et al., "Numerical simulation of composite-material rod-like jet penetrates underwater targets," *Explosive Materials*, vol. 48, no. 01, pp. 8-14, 2019.

[8] Z. Y. Gao, Z. X. Huang, M. Guo et al., "Anti-penetration performance analysis of diesel filled closed structures against shaped charge jet," *Journal of Vibration and Shock*, vol. 35, no. 14, pp. 176-181, 2016, doi: 10.13465/j.cnki.jvs.2016.14.029

[9] C. F. Zhao, X. D. Zu, "Effect of liquid density on the performance of unit cell structure in jet penetration resistance," *Journal of Projectiles, Rockets, Missiles and Guidance*, vol. 38, no. 01, pp. 65-68, 2018, doi: 10.15892/j.cnki.djzdxb.2018.01.016

[10] C. F. Zhao, X. D. Zu, "Study on the effect of liquid sound velocity on the anti-jet penetration performance of unit cell structure," *China Sciencepaper*, vol. 12, no. 22, pp. 2565-2568, 2017, doi: 10.3969/j.issn.2095-2783.2017.22.009

[11] C. F. Zhao, F. Shan, J. Yu et al., "Effect of structural shape on the penetration resistance of closed cell," *Blasting*, vol. 23, no. 6, pp. 22-25, 2017.

[12] C. F. Zhao, C. R. Liu, "Effect of dynamic viscosity on jet penetration resistance of liquid composite cell," *Ordnance Material Science and Engineering*, vol. 41, no. 06, pp. 88-91, 2018, doi: 10.14024/j.cnki.1004-244x.20181015.002

[13] C. F. Zhao, J. Ren, T. F. Kuai, et al., "Theoretical analysis of residual head velocity after the jet penetrating the multi-layer metal-liquid composite structure," *2019 International Conference on Optoelectronic Science and Materials, Hefei, China. IOP Conference Series: Materials Science and Engineering*, vol. 711, no. 012061, 2020, doi: 10.1088/1757-899X/711/1/012061

[14] F. Shan, C. F, Zhao, X. D. Zu, "Effect of size effect on jet penetration resistance of closed structure," *Journal of Ordnance Equipment Engineering*, vol. 39, no. 03, pp. 68-71, 2018.

[15] C. X. Zhao, F. C. Yin, "Analysis of anti-jet penetration characteristics of axial single-cell/multi-cell closed structure," *Proceedings of 2019 2nd International Conference on Advanced Electronic Materials, Computers and Materials Engineering, IOP Conference Series: Materials Science and Engineering*, vol. 563, no. 032035, 2019, doi: 10.1088/1757-899X/563/3/032035

[16] M. Guo, X. D. Zu, X. J. Shen et al., "Study on liquid-filled structure target with shaped charge vertical penetration," *Defence Technology*, vol. 15, no. 6, pp. 861-867, 2019, doi: 10.1016/j.dt.2019.05.003

[17] X. D. Zu, W. Dai, Z. X. Huang et.al., "Effects of liquid parameters on liquid-filled compartment structure defense against metal jet," *Materials*, vol. 12, no. 1809, pp. 1-14, 2019, doi: 10.3390/ma12111809

[18] Q. Zhang, R. J. .Zhang, "Numerical simulation of explosion using ALE method," *Chinese Quarterly of Mechanics*, vol. 26, no. 4, pp. 639-642, 2005.

[19] C. B. Yao, H. B. Zhang, X. F. Pu et al., "Application of ALE method in numerical simulation of explosion dynamics," *Progress Report on China Nuclear Science and Technology-Proceedings of the 2009 Annual Conference of the Chinese Nuclear Society*, vol. 1, no. 6, pp. 155-159, 2009.

[20] B. M. Dobratz, P. C. Crawford, "LLNL explosive handbook: Properties of chemical explosives and explosive simulants," *Livermore, CA, US :Lawrence Livermore National Laboratory*: pp. 21-29, 1985.

[21] C. L. Jia, F. R. Chen, "Finite element simulation of Johnson-Cook constitutive model for 7A52 aluminum alloy," *Ordnance Material Science and Engineering*, vol. 41, no. 01, pp. 30-33, 2018, doi: 10.14024/j.cnki.1004-244x.20180105.001

[22] J. Xun, Z. Yang, Q. Li, "Simulation for submarine bullet's exterior ballistic based on dyna," *Fire Control & Command Control*, vol. 41, no. 03, pp.5-7, 2016, doi: 10.3969/j.issn.1002-0640.2016.03.002

[23] X. Zhang, X. D. Zu, Z. X. Huang et al., "Analysis of liquid-filled unit cell structure subjected to shaped charge jet impact," *Explosion and Shock Waves*, vol. 37, no. 06, pp. 1101-1106, 2017.